Combined effects of elevated temperatures and high strain rates on compressive performance of S30408 austenitic stainless steel

Li, Lijun; Wang, Rui; Zhao, Hui; Zhang, Haoran; Yan, Rui

DOI
10.1016/j.istruc.2021.07.063

Publication date
2021

Document Version
Accepted author manuscript

Published in
Structures

Combined effects of elevated temperatures and high strain rates on compressive performance of S30408 austenitic stainless steel

Lijun Li [a], Rui Wang [a], Hui Zhao [a, b*], Haoran Zhang [a], Rui Yan [c]

Submitted to: Structures

[a]College of Civil Engineering, Taiyuan University of Technology, Taiyuan, China;
[b]Department of Civil Engineering, Tianjin University, Tianjin, China;
[c]Faculty of Civil Engineering and Geosciences, Delft University of Technology, Netherlands

---

* Corresponding author:
Hui Zhao
Tel: +86 351 6010280
Email: zhaohui01@tyut.edu.cn

Abstract:

304 austenitic stainless steel (ASS) has been increasingly utilized in engineering structures. However, the lack of study on this type of steel under extreme conditions restricts its application. Hence, this paper presents an experimental investigation of the combined influences of elevated temperatures and high strain rates on the mechanical performance of S30408 ASS, which is essential for determining the behaviour of structures made with this type of steel subjected to the coupled fire and impact/explosion. For this purpose, the quasi-static and dynamic compression tests using Split Hopkinson Pressure Bar (SHPB) were conducted under temperatures of 20-600 ºC and strain rates from 0.001 to 3000 s^{-1}. In addition, the corresponding microstructures of tested samples were observed. The stress-strain responses, strain rate and temperature effects as well as the microstructural evolutions were analyzed. Test results show that the stress-strain responses are sensitive to the strain rate and temperature. The strain-rate sensitivity coefficient increases as the strain rate and temperature rise. The microstructural observation reveals that the grain dimension declines with an increment of strain rate or a decreasing temperature. Finally, the dynamic compressive stress-strain models for S30408 ASS under elevated temperatures were suggested on the basis of the Johnson-Cook (J-C) model and have been proved to give a reasonable prediction.

Keywords: S30408 austenitic stainless steel; Elevated temperatures; Dynamic response; Strain rate; Constitutive model.

1. Introduction

In the last decades, 304 austenitic stainless steel (ASS) has been increasingly used in engineering structures [1-6]. It has several advantages compared to carbon steel, such as high corrosion resistance and durability, maintenance, improved fire and impact/blast resistance, etc. Due to these benefits, it is expected to be widely employed in the modern construction field, especially considering the life-cycle cost. Several design codes have been developed to regulate the use of the stainless steel in civil engineering, such as CECS 410:2015 [7] and EN 1993-1-4 [8]. Until now, the material and structural behaviours of 304 ASS subjected to the single static, dynamic, cyclic and fire conditions are relatively well understood [1-6, 9-20]. In addition to the loading conditions mentioned above, the structures may suffer combined fire and impact/explosion action during the lifetime [21, 22], such as 9.11 terrorist attack and Qingdao pipeline leak explosion. The fire may easily results in an explosion or progressive collapse, as presented in Fig. 1. Therefore, it is essential to systematically investigate the mechanical performance and microstructural characteristic of 304 ASS exposed to both high temperatures and strain rates in order to ensure the safety of 304 ASS structures subjected to such harsh environment.

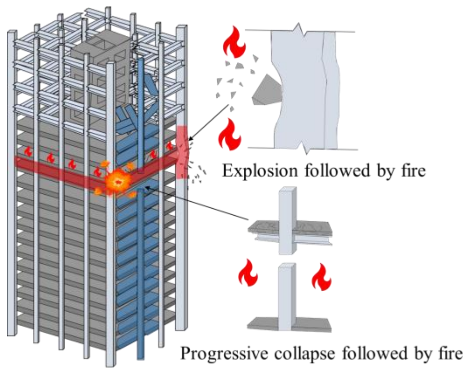

Fig. 1. Schematic view of explosion or progressive collapse followed by a fire.

For 304 ASS, the quasi-static mechanical performance at elevated temperatures and the dynamic mechanical properties at ambient temperature have been extensively examined [9, 10, 16, 18]. Results demonstrate that temperature causes a significant decrease in material strength, whereas the high strain rate induces a strengthening effect on the yield stress at ambient temperature. EN 1993-1-2 [23] suggests that the nominal yield stress declines by about 50% when the temperature reaches 600°C. Compared to carbon steel, stainless steel presents better high-temperature performance. As for the effect of strain rate at ambient temperature, a pronounced increase in the nominal yield stress exists provided that the strain rates exceed 10^3 s^{-1}, owing to an enhanced rate of dislocation generation. Jia et al. [18] found that the dynamic yield strength of S30408 ASS under strain rate of 6212 s^{-1} can reach up to approximate 3 times of that under quasi-static load.

Current results indicate that the mechanical properties of stainless steel are temperature and strain rate sensitive. Given the coupled temperature and dynamic loadings, the strengthening induced by the high strain rate and the thermal softening may complicate the stress-strain responses. Though previous researches on the 304 ASS have covered material and structural levels, the information on the coupled influences of high strain rates and elevated temperatures is still limited. Lee et al. [24, 25] investigated the compressive performance and microstructure change of 304L ASS considering the influences of strain rate, temperature and pre-strain. Test strain rates and temperatures were set in the range of 2000-6000 s^{-1} and 300-800 °C, respectively. It is concluded that the strain-rate sensitivity increases with rising strain rates and the descending temperatures. The microstructural observation indicated that the change in the flow stress under combined high strain rates and temperatures is related to the quantity of martensite and the densities of both dislocation and twin. Cadoni and Forni [26] studied the influences of strain rate and temperature on the mechanical responses of cold-formed AISI 304 ASS bars. Experiments were conducted using a split-Hopkinson tension bar under temperatures up to 1000 °C and 3 strain rates (250, 400 and 800 s^{-1}). They found that the yield stress decreases with the increasing temperatures and increases with an increment of the strain rate. Finally, the parameters of the Johnson-Cook (J-C) and Cowper-Symonds (C-S) models were determined. In 2020, Yang et al. [27] conducted SHPB tests to analyze the influences of strain rate and temperature on the compressive performance of ASTM

A240/A240M 304 stainless steel. Due to the increased carbon content, the quasi-static yield stress achieves 702 MPa at room temperature. Additionally, the modified J-C model was suggested according to the test results. Table 1 summarizes the detailed information in literatures [24-27]. As mentioned previously, the existing researches are not sufficient to fully understand the performance of 304 ASS under combined high temperatures and high strain-rate conditions because of the different chemical compositions and test conditions.

Table 1

Detail information in literatures [24-27].

Sources	Type	Strain rate (s^{-1})	Temperature (°C)	Content
Lee et al. [24, 25]	Pre-strained 304L ASS bars	2000-4000, 4000-6000	300, 500, 800	Compressive stress-strain curves, microstructure
Cadoni and Forni [26]	AISI304 ASS bars in cold forming	250, 400, 800	200, 400, 600, 800, 1000	Tensile stress-strain curves, constitutive models
Yan et al. [27]	ASTM A240/A240M 304 ASS	1000, 3000, 5000	300, 500, 700	Compressive stress-strain curves, constitutive models

In this context, the quasi-static and dynamic compressive behaviours of a typical 304 ASS have been investigated under varying high temperatures (from 20 to 600 °C) and strain rates (0.001, 1000, 2000 and 3000 s^{-1}). The universal compression machine and SHPB tester equipped with an electric furnace were employed for the quasi-static and dynamic tests under elevated temperatures, respectively. The stress-strain responses, strain rate and temperature effects and microstructural changes were obtained and analyzed. Finally, the dynamic stress-strain model considering both the temperature and strain rate is developed on the basis of the J-C model. The above results can be used for evaluation of the structural safety when subjected an impact/explosion followed by a fire.

2. Experiments

2.1. Material and Sample preparation

The material investigated in this work was S30408 ASS with the following chemical composition: C(0.02%), S(0.002%), P (0.033%), Si(0.46%), Mn(1.35%), Cr(18.15%), Ni(8.06%), corresponding to 304 in ASTM [28] and 1.4301 in EN 10088-1 [29]. All samples for mechanical characterization were obtained from the steel tube in the longitudinal direction using the wire-cut electrical discharge machine. In order to achieve good flatness and parallelism, the ends of SHPB samples were polished using a series of sand papers (grit dimensions: 400 to 2000 mesh). The quasi-static tensile test was conducted at room temperature with a constant 0.001 s^{-1} strain rate, according to ISO 377:2013 [30]. The engineering stress-strain relationships are depicted in Fig. 2. Due to the unobvious yield plateau, the yield stress was taken as the 0.2% proof stress in accordance with GB/T 228.1-2010 [31]. The mean Young's modulus, yield strength, ultimate tensile strength and elongation are 191.4 GPa. 261.3 MPa, 611.2 MPa and 54%, respectively. According to GB/T 34108-2017 [32], samples for quasi-static and dynamic compression tests under elevated temperatures are cylindrical in shape with dimensions of Ø 5 mm×5 mm and Ø 8 mm×4 mm, respectively. A diameter to height ratio of 2 is designed in the dynamic compression samples to decrease the influences of friction and inertia.

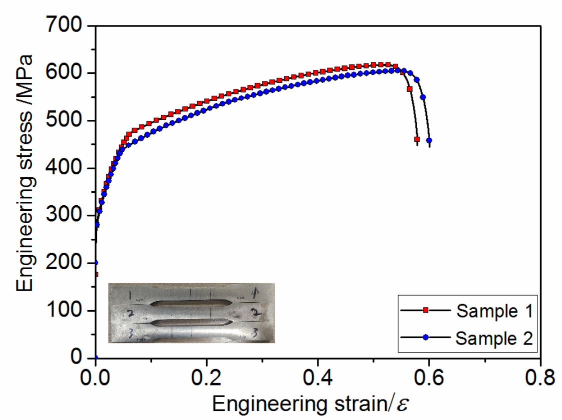

Fig. 2. Stress-strain responses of S30408 ASS under quasi-static tensile.

2.2. Experimental setup and procedure

2.2.1 Quasi-static compression under elevated temperatures

A quasi-static compression test can serve as a basis for assessing the thermal and strain-rate effects. A total of 12 samples were tested in a quasi-static compression regime using a 30 kN universal compression machine equipped with an electric furnace, as presented in Fig. 3. Two high-temperature resistance and high strength ceramic bars were installed to transfer the load from the testing machine to the sample. The thermocouple wire was wrapped around the sample to monitor the temperature.

Samples were first heated to the target temperatures (200, 400 and 600 $^{\circ}$C) with the speed of 2 $^{\circ}$C/min. Then, in order to ensure a homogenous temperature within the samples, the target temperatures were held for 5 min. Finally, the samples were compressed with the rate of 0.3 mm/min to failure in a steady-state condition. The corresponding load and deformation were automatically obtained. At least three tests were performed for each strain rate and temperature, and final results were the average value of three samples.

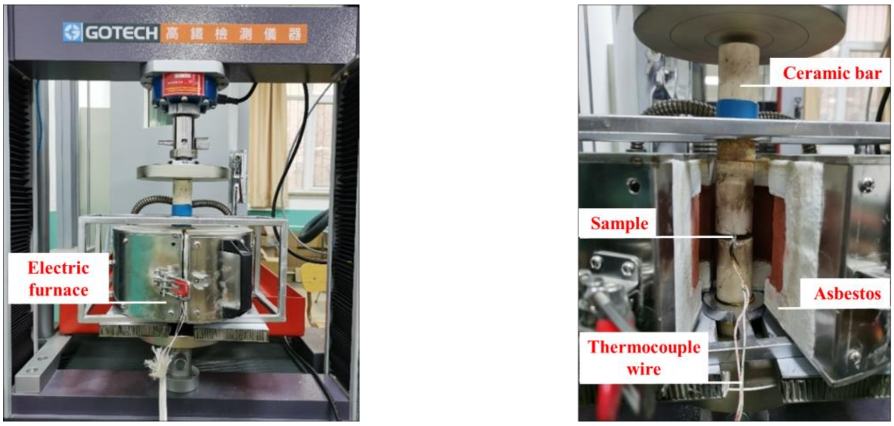

(a) Whole apparatus (b) Internal state of the furnace

Fig. 3. Device for Quasi-static compression at elevated temperatures.

2.2.2 Dynamic test under elevated temperatures

It is known that the SHPB device is the most widely used to measure the dynamic mechanical properties of steel material. In this work, 36 dynamic tests were performed using an SHPB tester accompanying an electric oven with a 1200 $^{\circ}$C heating capacity. The equipment contains the air gun, strike, incident and transmitter bars, an energy-absorption apparatus and an oven. The photo and schematic view are shown in Fig. 4. The incident and transmitter bars, which are 1200 mm in length and 14 mm in diameter, are produced with 18Ni steel. The longitudinal wave speed and the Young’s modulus of 18Ni steel are 5092 m/s and 210 GPa, respectively. At room temperature, the molybdenum disulfide was adopted between the contact surfaces of the sample and the bars to decrease the friction, and a copper pulse shaper was placed at the impact end of the incident bar to produce a stable wave [33]. A synchronically assembled furnace was designed to heat the sample while keeping the SHPB bars away from it to avoid the influence of elevated temperatures on the bars. The thermocouple was attached to the sample to measure the sample's temperature.

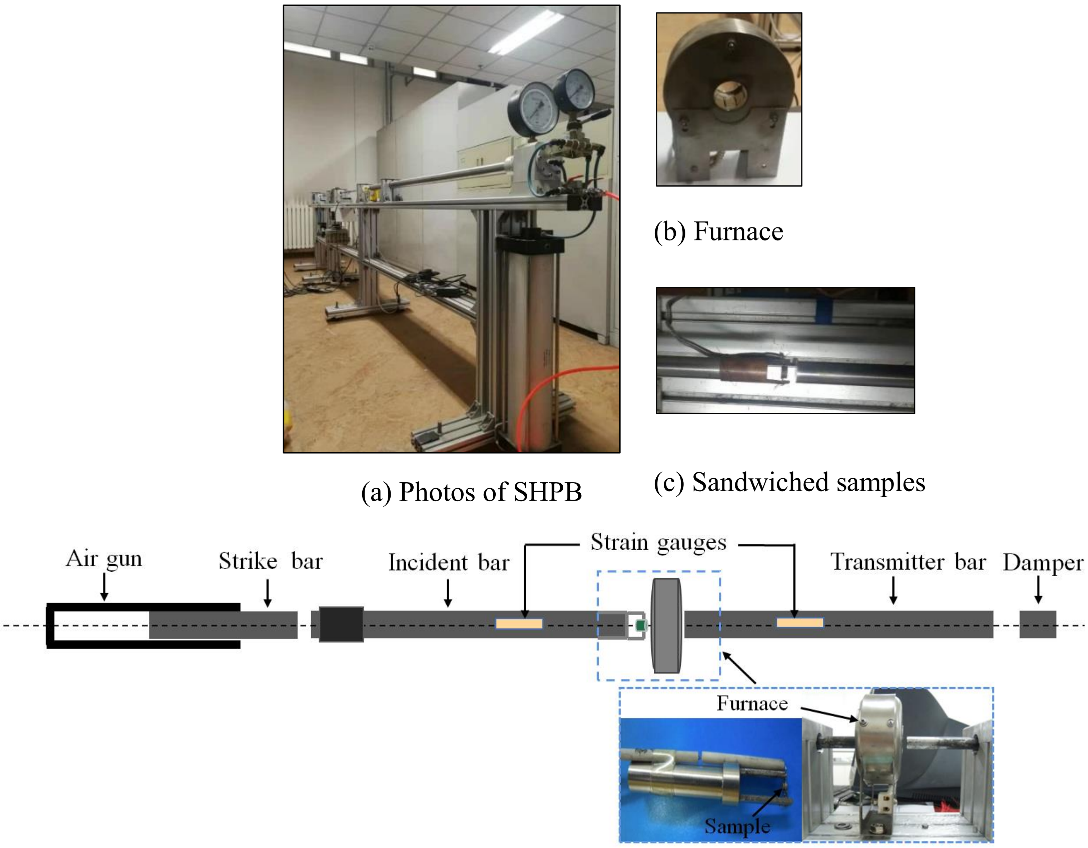

Fig. 4. Set-up for dynamic tests under elevated temperatures.

The experiments were performed as follows: (1) Firstly, the samples were mounted with a thermocouple sleeve and heated at a speed of 2 ºC/min to the predetermined temperature followed by 5 min to achieve a uniform temperature distribution in the samples; (2) Secondly, the bars were brought into contact with the sample, and then the strike bar was fired. A similar method was also used in other high-temperature SHPB test [34]. The incident, transmitter and reflection strain waves (ε_I, ε_T and ε_R) were detected by the strain gauges. Based on the uniaxial elastic wave theory, the engineering strain (ε_{eng}), engineering stress (σ_{eng}) and strain rate ($\dot{\varepsilon}$) can be calculated by Eqs. (1)-(3), respectively.

$$\varepsilon_{\mathrm{eng}} = -\frac{2C_0}{L}\int_0^{\mathrm{t}} \varepsilon_{\mathrm{R}}\,\mathrm{d}t \tag{1}$$

$$\sigma_{\mathrm{eng}} = E_0 \cdot \frac{A_0}{A_{\mathrm{s}}} \cdot \varepsilon_T \tag{2}$$

$$\dot{\varepsilon} = -\frac{2C_0}{L} \cdot \varepsilon_{\mathrm{R}} \tag{3}$$

in which C_0 represents the velocity of the bar elastic wave, A_s and L denote the cross-sectional area and the gauge length of the sample, respectively; E_0 and A_0 represent the Young's modulus and cross-sectional area of the bars. The true strain (ε_{true}) and true stress (σ_{true}) are evaluated as follows:

$$\varepsilon_{\mathrm{true}} = -\ln(1-\varepsilon_{\mathrm{eng}}) \tag{4}$$

$$\sigma_{\mathrm{true}} = \sigma_{\mathrm{eng}}(1-\varepsilon_{\mathrm{eng}}) \tag{5}$$

The dynamic tests were conducted at temperatures of 20, 200, 400 and 600 ºC, respectively, and averaged strain rates of 1000, 2000 and 3000 s^{-1}. Three samples were tested at each temperature and strain rate.

2.2.3 Microstructure analysis

The microstructures of the samples after both elevated temperature and impact loadings were examined using the optical microscope (Primotech, Zeiss). The samples were inlaid with a metallographic inlay machine and polished using sandpapers and polishing machine, and then etched with the aqua regia through repeated wiping. When the surface colour changes to brown, C_2H_5OH was immediately used to clean the samples for around 30 s.

3. Results and analysis

3.1. Stress-strain response

As mentioned above, the dynamic stress-strain responses were calculated based on the strain pulses in the SHPB tests. The typical incident, reflected and transmitted strain waves (ε_I, ε_R and ε_T) are given in Fig. 5(a). In order to verify the stress equilibrium, the time histories of $\varepsilon_I+\varepsilon_R$ and ε_T are depicted in Fig. 5(b). As shown, the $\varepsilon_I+\varepsilon_R$ is approximately equal to ε_T under dynamic loading, which indicates that the samples are at a stress equilibrium state and the test results are reliable. It is known that keeping the strain rate constant is difficult when subjected to the quick loading. In general, the strain rate became relatively stable after experiencing the rapid-rise and obvious fluctuation stages, and similar trends were also found in other SHPB tests [35, 36]. Given the unstable strain rate over the whole period, the integral averaging method suggested by Yang et al. [35] is employed to calculate the strain rate in this work.

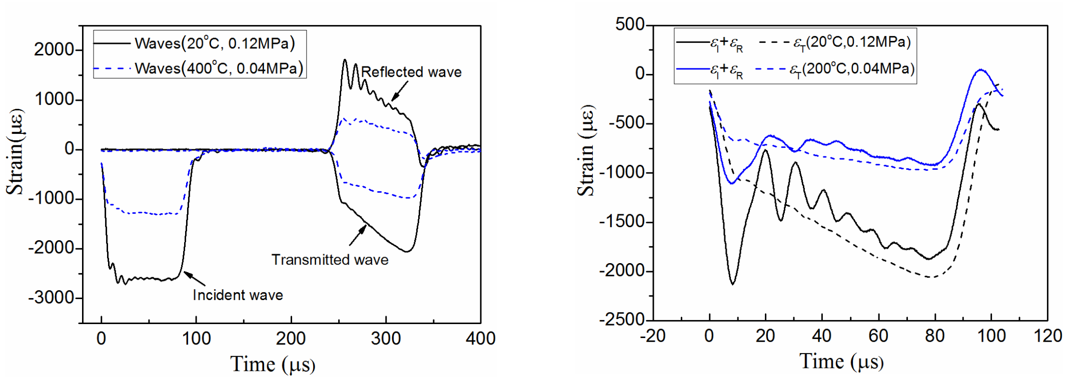

(a) Representative strain waves (b) Time histories of $\varepsilon_I+\varepsilon_R$ and ε_T

Fig. 5. Typical raw strain waves.

Fig. 6 presents the averaged true stress-strain responses of 3 repeated tests deformed under varying strain rates and temperatures. It is observed that the stress-strain curves significantly depend on the strain rates and temperatures. The flow stresses rise with the increasing strain rates, but an increment of temperature results in a decreasing flow stress. In addition, the stress-strain responses present a work-hardening behaviour with the increasing strains, and the rate of the working-hardening declines with an increment of temperature. In the subsequent analysis, the influences of temperature and strain rate on the yield stresses will be examined.

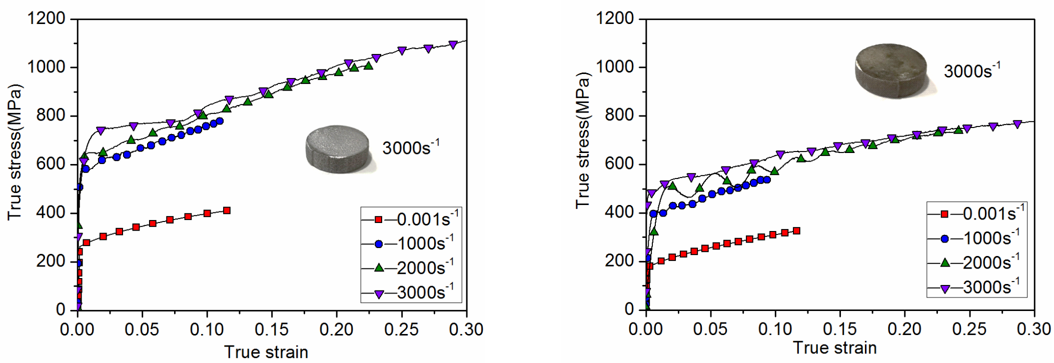

(a) 20 °C (b) 200 °C

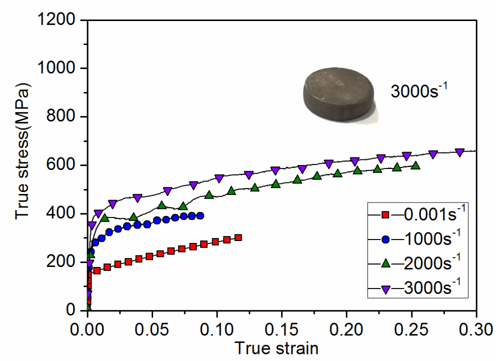

(c) 400 ºC

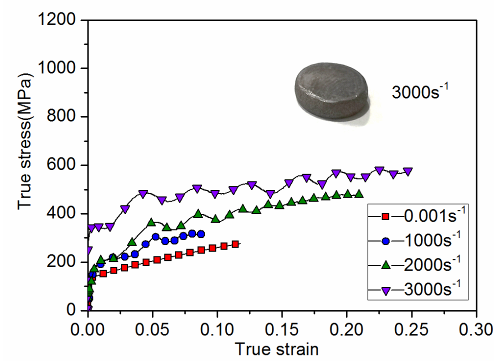

(d) 600 ºC

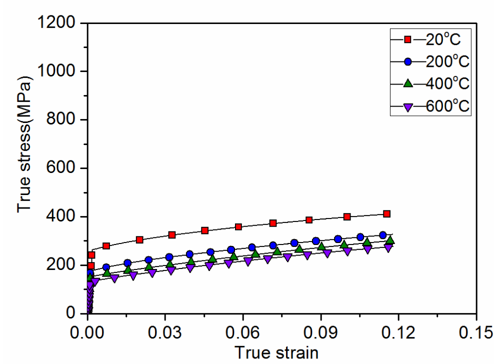

(e) 0.001 s^{-1}

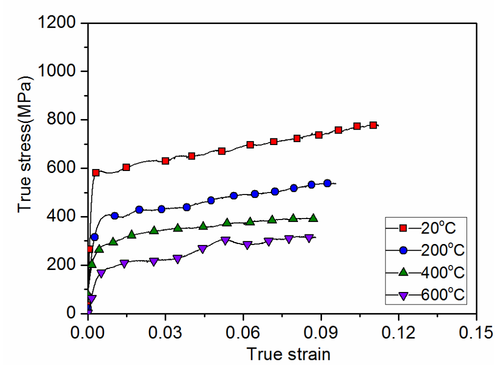

(f) 1000 s^{-1}

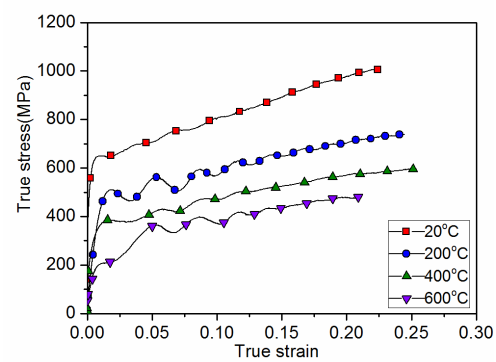

(g) 2000 s^{-1}

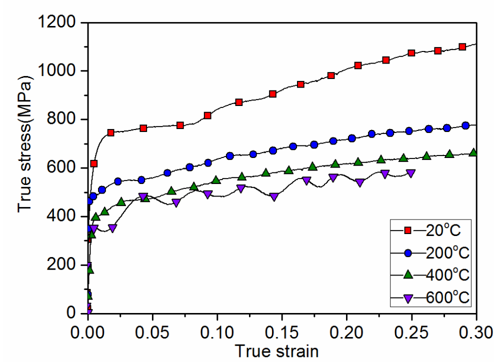

(h) 3000 s^{-1}

Fig. 6. True stress vs. strain responses.

3.2. Influences of strain rate and temperature

The variations of yield stresses along with the strain rate and temperature are presented in Figs. 7(a) and 7(b), respectively. Since the elastic part of the stress-strain response is fluctuating, the method for extracting the dynamic yield stress is different from that adopted in the quasi-static test. Thus, the method recommended by Yang et al. [35] and Sun and Packer [37] was employed to define the dynamic yield stress, as presented in Fig. 8. It can be seen in Fig. 7 that the yield stresses are sensitive to the strain rate and temperature. For a given strain rate, the yield stress declines when the temperature increases. However, it rises with an increment of strain rate when subjected to the same temperature.

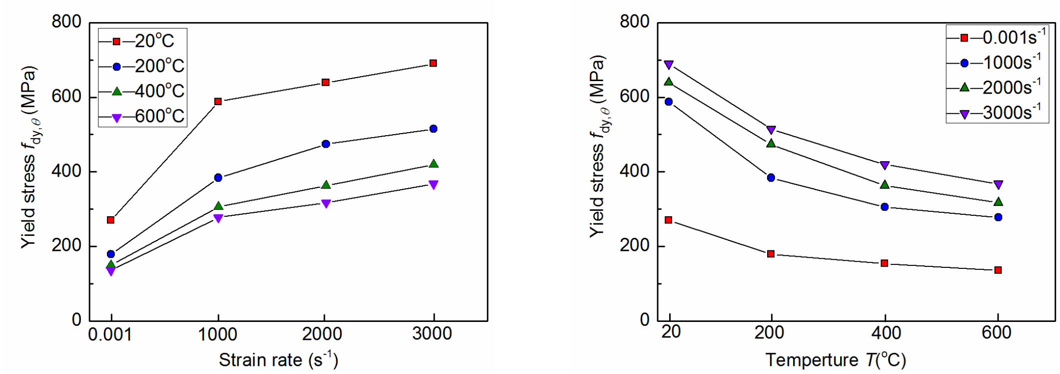

(a) Yield stress versus strain rate (b) Yield stress versus temperature

Fig. 7. Variations of yield stresses with the strain rate and temperature.

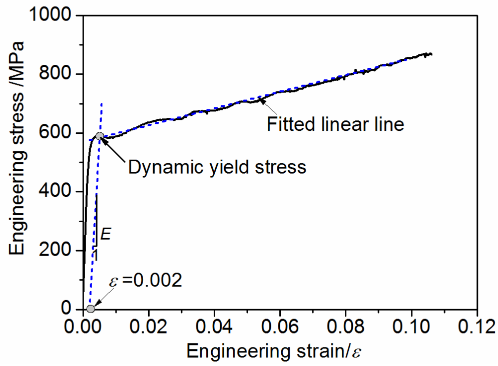

Fig. 8. Definition of dynamic yield stress.

In order to quantify influences of strain rate and temperature on the dynamic compression response, the dynamic increase factor $\mathrm{DIF}_{\mathrm{dy},\theta}$ and temperature reduction coefficient $k_{\mathrm{dy},\theta}$ of the yield stress subjected to varying strain rates and temperatures are presented in Figs. 9(a) and 9(b), respectively. The corresponding formulas are given as follows:

$$\mathrm{DIF}_{\mathrm{dy},\theta}=f_{\mathrm{dy},\theta}\,/\,f_{\mathrm{sy},\theta} \tag{6}$$

$$k_{\mathrm{dy},\theta}=f_{\mathrm{dy},\theta}\,/\,f_{\mathrm{dy},20^{\circ}\mathrm{C}} \tag{7}$$

in which $f_{\mathrm{dy},\theta}$ and $f_{\mathrm{dy},20^{\circ}\mathrm{C}}$ are the dynamic yield stresses at elevated temperatures and ambient temperature, respectively; $f_{\mathrm{sy},\theta}$ represent the quasi-static yield stress under elevated temperatures.

The developments of $\mathrm{DIF}_{\mathrm{dy},\theta}$ with increasing strain rates under 20, 200, 400 and 600 °C are depicted in Fig. 9(a). As presented, the $\mathrm{DIF}_{\mathrm{dy},\theta}$ values under high-strain rates are greater than 1.0. In general, the highest values appear at 200 °C. The increase rate of the yield stress from 0.001 to 1000 s^{-1} is higher than that in the range of 1000-2000 s^{-1} and 2000-3000 s^{-1}. For instance, under 400 °C exposure, the yield stresses at strain rates of 1000, 2000 and 3000 s^{-1} increased by 99%, 136% and 173%, respectively, compared to that under quasi-static strain rate. It indicates that the strengthening effect is pronounced under a high strain rate compared with the quasi-static condition. The evolution of $DIF_{dy,\theta}$ in this work is also compared with literature results, as illustrated in Fig. 9(a). The $DIF_{dy,\theta}$ values derived from the results of Lee and Lin [9] are close to those obtained in this work, while the results of Jia et al. [38] under temperatures of 172 °C are relatively low. The above results indicate that the yield stresses of S30408 ASS present an obvious strain-rate effect.

The reduction factors $k_{dy,\theta}$ induced by the same temperature were higher under 2000 s^{-1} and 3000 s^{-1} than the rest, as presented in Fig. 9(b). There are 2 phases for the yield strength degradation. The yield strength degrades fastly during 20-200 °C and gradually decline between 200 °C and 600 °C. When subjected to 200, 400 and 600 °C, the retained yield strengths under different strain rates are in the range of 65-75%, 52-61% and 47-53% of the values at ambient temperatures, respectively. Fig. 9(b) also compares the reduction factor of austenitic stainless steel suggested by Fan et al. [16] and EN 1993-1-2 [23] under the quasi-static loading. These two models are found to give reasonable predictions of the residual dynamic yield stress under varying temperatures, considering the variability in high-temperature tests.

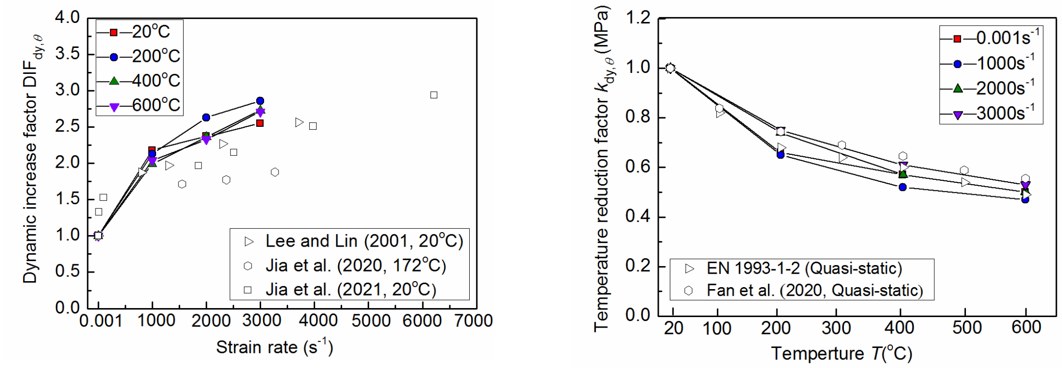

(a) $DIF_{dy,\theta}$ (b) $k_{dy,\theta}$

Fig. 9. Dynamic increase factors $DIF_{dy,\theta}$ and temperature reduction coefficients $k_{dy,\theta}$

For each temperature, the influence of the strain rate on the compressive performance can be qualified via the strain-rate sensitivity coefficient β [18], defined as:

$$\beta=(\ln\sigma_2-\ln\sigma_1)/(\ln\dot{\varepsilon}_2-\ln\dot{\varepsilon}_1) \quad (8)$$

in which σ_1 and σ_2 represent the true stresses at 0.05 strain corresponding to the strain rates $\dot{\varepsilon}_1$ and $\dot{\varepsilon}_2$, respectively. The greater value of β indicates more sensitivity to the strain rate. Fig. 10 presents the variation of parameter β with the strain rate under different temperatures. The parameter β increases when the strain rate rises, ranging from 0.03 to 0.4. As the strain rate exceeds 1000 s^{-1}, higher temperature induces the greater value of β, especially for 400 and 600 ºC.

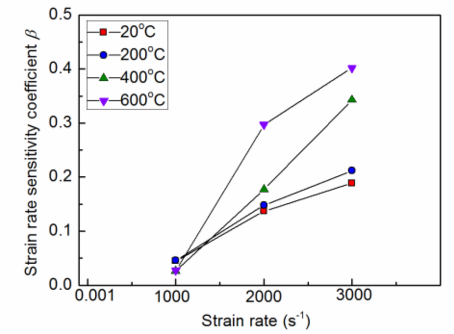

Fig. 10. Strain-rate sensitivity coefficient

3.3. Strain rate models

Test results have indicated that the stress-strain responses of S30408 ASS are related to the strain rate and the temperature. Therefore, a widely used temperature and rate dependence model, called the J-C model [39], is employed to predict the true stress-strain responses. This model is embedded in the finite element software by considering the influences of the strain hardening, strain rate strengthening and temperature softening, which can be written as follows:

$$\sigma=(A+B\varepsilon_p^n)(1+c\ln(\frac{\dot{\varepsilon}}{\dot{\varepsilon_0}}))(1-T^{*m}) \tag{9}$$

in which ε_p represents the true plastic strain; $\dot{\varepsilon}$ and $\dot{\varepsilon_0}$ are strain rate and quasi-static strain rate(=0.001 s^{-1}), respectively; T* represents the homologous temperature (=$(T$-$T_r)/(T_m$-$T_r)$, T, T_r and T_m denote current temperature, ambient temperature and melting temperature, respectively); Parameters A, B and n denote the quasi-static stress-strain response at room temperature; Parameters c and m denote the strain-rate strengthening and thermal softening effects, respectively. Therefore, these 3 parts in each bracket are uncoupled in the model.

It should be noted that during SHPB tests, a temperature increment occurs due to the plastic deformation, which is recognized as the adiabatic process. The temperature rise results in the thermal softening and becomes more obvious under higher strain rate. Thus, the adiabatic temperature increment ΔT is considered in J-C model, as calculated by Eq.(10):

$$\Delta T = \frac{\beta}{\rho c_{\mathrm{p}}} \int \sigma(\varepsilon) \mathrm{d}\varepsilon \tag{10}$$

in which β represents the Taylor-Quineey factor taken as 0.9 in this work according to [26], ρ denotes the density (7.9 g/cm^3), c_{p} is the heat capacity (500 J kg^{-1}K^{-1}).

By using Eq. (10), taking S30408 ASS under 3000 s^{-1} and 200 °C as an example, the temperature increments achieve 51.5 °C at strain of 0.3. Therefore, the temperature rise caused by the adiabatic process should be incorporated in the model, especially at higher strain rate.

The five parameters are determined by the test results fitting and their values are presented in Table 2, in which different values of m are given corresponding to different temperatures. Fig. 11 presents the comparison between the model and test curves. In general, the model shows a reasonable agreement with the test data. Some discrepancies between test and predicted results are mainly related to some factors, such as the microstructural transformation, the adiabatic heat softening and the experimental error, etc [18, 38, 40].

Table 2

Fitted J-C parameters.

A(MPa)	*B*(MPa)	*n*	*c*	*m*		
				200°C	400 °C	600 °C
270	637	0.7587	0.0959	0.538	0.653	0.808

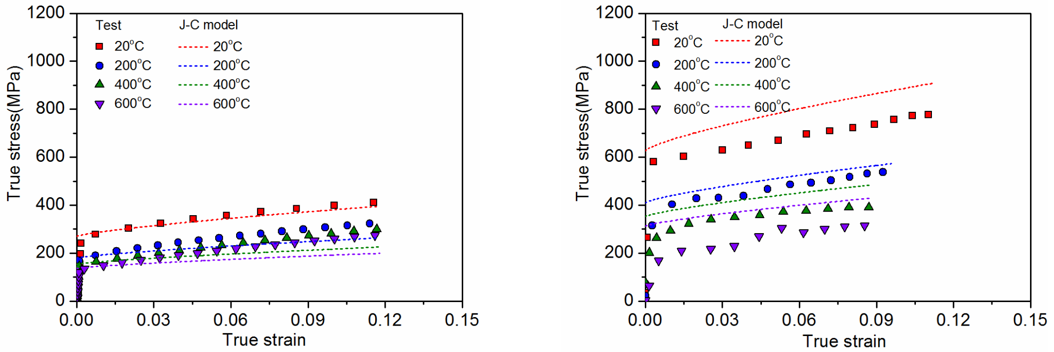

(a) 0.001 s^{-1} (b) 1000 s^{-1}

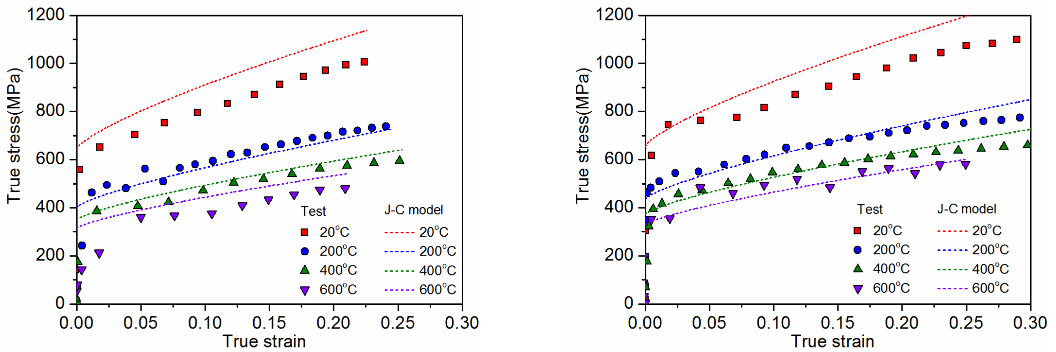

(c) 2000 s^{-1} (d) 3000 s^{-1}

Fig. 11. Comparison between the test results and J-C model

3.4. Microstructural observation after elevated-temperature dynamic test

After compression deformation, the microstructures were examined using the optical microscopy to analyze the relationship between the elevated-temperature dynamic properties and the residual microstructure, as presented in Fig. 12. The photographs show that a higher temperature results in a pronounced increase in the grain sizes and a decline of the grain boundary area when exposed to the same strain rate. Considering that the grain boundary hinders the plastic deformation and has higher strength than the inner grain, the smaller the grain boundary area is, the lower the strength and hardness are. Therefore, the inferior mechanical responses of S30408 ASS were obtained at higher temperatures. In addition, as the strain rate increases, the average grain dimension decreases while the grain boundary gradually diffuses and become irregular. Therefore, the rise in the grain boundary area under a higher strain rate benefits the mechanical performance. In general, the grains maintain a well integrity structure, and the changes in the grain shape are unobvious under varying temperatures and strain rates, indicating a good performance of S30408 ASS under coupled fire and impact loadings.

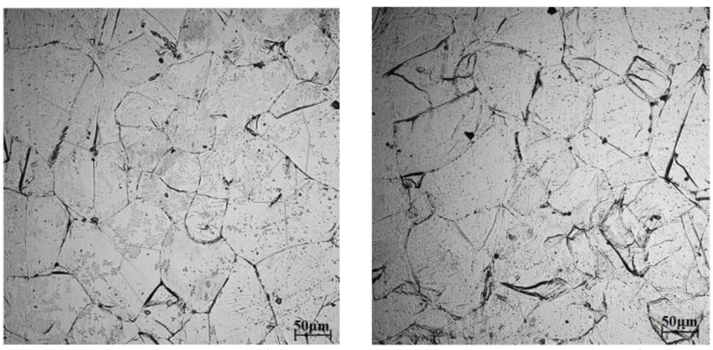

(a) 20°C, 3000s^{-1} (b) 200 °C,3000s^{-1}

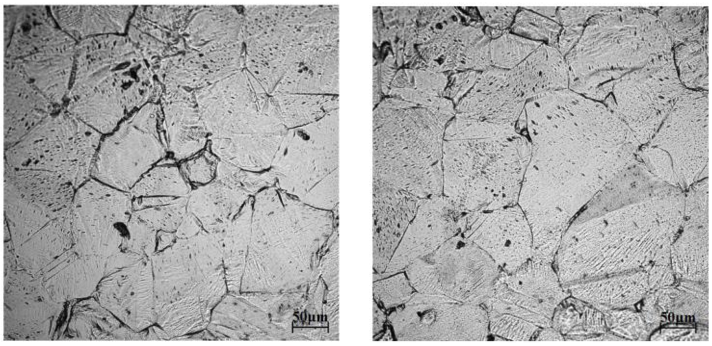

(c) 400 °C, 3000s^{-1} (d) 600 °C, 3000s^{-1}

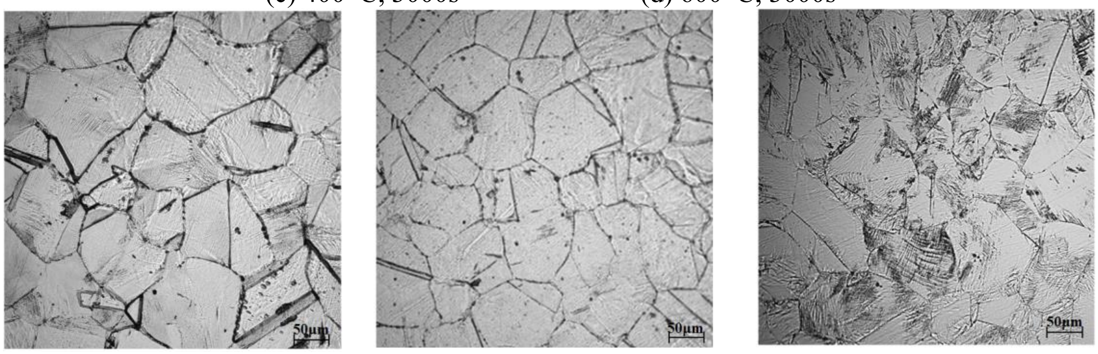

(e) 20 °C, 1000s^{-1} (f) 20 °C, 2000s^{-1} (g) 20 °C, 3000s^{-1}

Fig. 12. Optical microstructures under different strain rates and temperatures.

4. Conclusions

This study investigated the quasi-static and dynamic compressive behaviours of S30408 austenitic stainless steel (ASS) under elevated temperatures of 20, 200, 400 and 600 °C and strain rates ranged from 0.001 s^{-1} to 3000 s^{-1}. According to the test and analyses, the main conclusions are obtained:

(1) The compressive responses of S30408 ASS are sensitive to the strain rate and temperature. The yield stress increases with an increment of the strain rate, but declines with increased temperatures. In addition, the rate of the working-hardening becomes weaker at higher temperatures.

(2) As the strain rate rises from 0.001 s^{-1} to 3000 s^{-1}, the elevated-temperature dynamic increase factors $\mathrm{DIF}_{\mathrm{dy},\theta}$ rises, with the maximum value of 2.86 under 200 °C and 3000 s^{-1}. The temperature reduction coefficients $k_{\mathrm{dy},\theta}$ decreases significantly during 20-200 °C and the reduction slows down from 200 to 600 °C. The strain-rate sensitivity coefficient is more pronounced under a higher strain rate and a higher temperature.

(3) Based on the experimental results, the parameters for J-C constitutive model were

determined. This model could be used to predict the residual performance of structures made with this type of steel under the coupled action of fire and impact/blast loadings.

(4) Residual microstructure indicates that higher temperatures result in an obvious rise of the grain size, while the increase in the strain rate decreases the grain size. In general, the moderate grain deformation occurs under coupled high temperatures and strain rates within the parameter range in this work.

Acknowledgements

The study was supported by the China Postdoctoral Science Foundation (2020M670656) and Fund Program for the Scientific Activities of Selected Returned Overseas Professionals in Shanxi Province (20210010).

References

[1] L.H. Han, C.Y. Xu, Z. Tao, Performance of concrete filled stainless steel tubular (CFSST) columns and joints: Summary of recent research, J. Constr. Steel Res. 152 (2019) 117-131.

[2] H. Zhao, R Wang, C.C. Hou, D. Lam, Performance of circular CFDST members with external stainless steel tube under transverse impact loading, Thin-Walled Struct. 145 (2019) 106380.

[3] S.K. Azad, D.X. Li, B. Uy, Axial slenderness limits for austenitic stainless steel-concrete composite columns, J. Constr. Steel Res. 166 (2020) 105856.

[4] M. Kucukler, Z. Xing, L. Gardner, Behaviour and design of stainless steel I-section columns in fire, J. Constr. Steel Res. 165 (2020) 105890.

[5] I. Arrayago, K.J.R. Rasmussen, E. Real, Statistical analysis of the material, geometrical and imperfection characteristics of structural stainless steels and members, J. Constr. Steel Res. 175 (2020) 106378.

[6] H. Zhao, R Wang, D. Lam, C.C. Hou, R Zhang, Behaviours of circular CFDST with stainless steel external tube: Slender columns and beams, Thin-Walled Struct. 158 (2021) 107172.

[7] CECS 410: 2015, Technical Specification for Stainless Steel Structure, Planning Press of

China, Beijing, 2015 (In Chinese).

[8] EN 1993-1-4:2006+A1: 2015. Eurocode 3—Design of Steel Structures Part1–4: General Rules-Supplementary Rules for Stainless Steel. British Standards Institution. London, UK, 2015.

[9] W.S. Lee, C.F. Lin, Impact properties and microstructure evolution of 304L stainless steel, Mater. Sci. Eng. A. 308(2001) 124-135.

[10] J.A. Lichtenfeld, C.J.V. Tyne, M.C. Mataya, Effect of strain rate on stress-strain behavior of alloy 309 and 304L austenitic stainless steel, Metall. Mater. Trans. A. 37 (2006) 147-161.

[11] F. Zhou, B. Young, Experimental and numerical investigations of cold-formed stainless steel tubular sections subjected to concentrated bearing load, J. Constr. Steel Res. 63(11)(2007) 1452-1466.

[12] K. Abdella, Explicit full-range stress-strain relations for stainless steel at high temperatures, J. Constr. Steel Res. 65 (2009) 794-800.

[13] E. Cadoni, L. Fenu, D. Forni, Strain rate behaviour in tension of austenitic stainless steel used for reinforcing bars, Constr. Build. Mater. 35 (2012) 399-407.

[14] F. Zhou, L. Li, Experimental study on hysteretic behavior of structural stainless steels under cyclic loading, J. Constr. Steel Res. 122(2016) 94-109.

[15] M.J. Liu, S.G. Fan, R.M. Ding, G.Q. Chen, E.F. Du, K. Wang, Experimental investigation on the fire resistance of restrained stainless steel H-section columns, J. Constr. Steel Res. 163(2019) 105770.

[16] S.G. Fan, R.M. Ding, J.C. Zheng, F.Z. Xie, Refined model for the stress-strain curve of austenitic stainless-steel materials at elevated temperatures, J. Mater. Civ. Eng. 32 (4) (2020) 04020032.

[17] D. Fernando, J.G. Teng, W.M. Quach, L.D. Waal, Full-range stress-strain model for stainless steel alloys, J. Constr. Steel Res. 173(2020) 106266.

[18] S.G. Jia, Q.H. Tan, J.Y. Ye, Z.W. Zhu, Z.G. Jiang, Experiments on dynamic mechanical properties of austenitic stainless steel S30408 and S31608, J. Constr. Steel Res. 179(2021) 106556.

[19] A.D. Martins, R. Gonçalves, D. Camotim, Numerical simulation and design of stainless steel columns under fire conditions, Eng. Struct. 229(2021) 111628.

[20] H.X. Yuan, X.H. Liu, J.L. Liu, M. Theofanous, Cyclic behaviour and hysteretic model of austenitic stainless steel bolted T-stubs, J. Constr. Steel Res. 182 (2021) 106659.

[21] D. Forni, B. Chiaia, E. Cadoni, High strain rate response of S355 at high temperatures, Mater. Des. 94(2016) 467-478.

[22] E. Cadoni, D. Forni, Mechanical behaviour of a very-high strength steel (S960QL) under extreme conditions of high strain rates and elevated temperatures, Fire Saf. J. 109(2019) 102869.

[23] BS EN 1993-1-2, Eurocode 3: Design of steel structures: Part 1-2: General rules-Structural fire design, BSI, London, 2005.

[24] W.S. Lee, C.F. Lin, T.H. Chen, M.C. Yang, High temperature microstructural evolution of 304L stainless steel as function of pre-strain and strain rate, Mater. Sci. Eng. A. 527(2010) 3127-3137.

[25] W.S. Lee, C.F. Lin, T.H. Chen, M.C. Yang, Effects of prestrain on high temperature impact properties of 304L stainless steel, J. Mater. Res. 25(4)(2010) 754-762.

[26] E. Cadoni, D. Forni, Austenitic stainless steel under extreme combined conditions of loading and temperature, J. Dynamic Behav. Mater. 5(3)(2019) 230-240.

[27] Q.S. Yan, C.X. Lv, B.W. Sun, L. Yang, Dynamic mechanical behavior at elevated temperatures and high strain rate of structural stainless steel used in civil engineering, J. Mater. Civ. Eng. 32 (5) (2020) 04020094.

[28] A1022/A1022M-16b, Standard specification for deformed and plain stainless steel wire and welded wire for concrete reinforcement. ASTM International, United States, 2016.

[29] EN 10088-1: 2014, Stainless steels-Part 1: List of stainless steels, European committee for standardization, Brussels, 2014.

[30] EN ISO 377:2013, Steel and steel products - location and preparation of samples and test pieces for mechanical testing, CEN, Brussels, 2013.

[31] GB/T 228.1-2010, Metallic materials-Tensile testing-Part 1 Method of test at room

temperature. China Architecture & Building Press, Beijing, China, 2010.

[32] GB/T 34108-2017, Code for metallic materials-high strain rate compression method at ambient temperature, Standards Press of China, Beijing, China, 2017.

[33] Y.X. Mei, H.Y. Ban, High strain rate behaviour of stainless-clad bimetallic steel, Eng. Struct. 207(2020) 110219.

[34] P. Ponnusamy, S.H. Masooda, D. Ruan, S. Palanisamy, R.A.R. Rashid, R. Mukhlis, N.J. Edwards, Dynamic compressive behaviour of selective laser melted AlSi12 alloy: Effect of elevated temperature and heat treatment, Addit. Manuf. 36 (2020) 101614.

[35] X.Q. Yang, H. Yang, S.M. Zhang, Rate-dependent constitutive model of S690 high-strength structural steel, Constr. Build. Mater. 198 (2019) 597-607.

[36] Y. Zhu, H. Yang, S.M. Zhang, Dynamic mechanical behavior and constitutive models of S890 high-strength steel at intermediate and high strain rates, J. Mater. Eng. Perform. 29(2020) 6727-6739.

[37] M. Sun, J.A. Packer, High strain rate behavior of cold-formed rectangular hollow sections, Eng. Struct. 62(2014) 181-192.

[38] B. Jia, A. Rusinek, R. Pesci, S. Bahi, R. Bernier, Thermo-viscoplastic behavior of 304 austenitic stainless steel at various strain rates and temperatures: Testing, modeling and validation, Int. J. Mech. Sci. 170(2020) 105356.

[39] G.R. Johnson, W.H. Cook, A constitutive model and data for metals subjected to large strains, high strain rates and high temperatures, Den Haag, The Netherlands Proceedings of the 7th International Symposium on Ballistics (1983), pp. 541-547.

[40] X.L. Fan, T. Suo, Q. Sun, T.J. Wang, Dynamic mechanical behavior of 6061 AL alloy at elevated temperatures and different strain rates, Acta Mech. Solida Sin. 26(2013) 111-120.